Investigation of the Hydrogen Embrittlement of API 5L Natural Gas Pipeline Steels

Lucas Teeter
National Energy Technology Laboratory
1450 Queen Avenue SW
Albany, OR 97321, USA

Zineb Belarbi
National Energy Technology Laboratory
1450 Queen Avenue SW
Albany, OR 97321, USA

NETL Support Contractor
1450 Queen Avenue SW
Albany, OR 97321, USA

NETL Support Contractor
1450 Queen Avenue SW
Albany, OR 97321, USA

Kyle Rozman
National Energy Technology Laboratory
1450 Queen Avenue SW
Albany, OR 97321, USA

Omer Dogan
National Energy Technology Laboratory
1450 Queen Avenue SW
Albany, OR 97321, USA

ABSTRACT

Hydrogen ions produced during corrosion or through hydrogen blending into natural gas pipelines can lead to the degradation of ductility of metals used in these transmission pipelines. The effect of hydrogen on the mechanical properties of pipeline steels was studied for three grades of API 5L steels: X56, X65, and X100. These steels are either commonly used in or considered for use in natural gas transmission pipelines which are being considered for use in hydrogen blending. These steels were subjected to constant strain rate tensile testing after charging with electrochemically generated hydrogen. This paper reports on work to extend the life of the natural gas pipeline network via understanding the effect of hydrogen embrittlement induced by corrosion processes.

Key words: hydrogen embrittlement; pipeline steel; natural gas

INTRODUCTION

Increased interest in hydrogen research in the U.S. is in part driven by the desire to reduce dependence on fossil fuels and decarbonize many energy sectors by blending hydrogen in existing natural gas pipelines. Typical acceptable ranges for end-use systems have been suggested as 5-20% hydrogen[1]. The primary benefit of blending hydrogen into existing natural gas pipelines will be reducing greenhouse gas emissions from utilizing low-carbon sourced hydrogen[1].

The natural gas pipeline network in the U.S. consists of more than 210 individual pipeline systems and approximately 3 million miles consisting of distribution mains, distribution service lines, and transmission lines[1–4]. This makes the U.S. natural gas pipeline network the most extensive pipeline delivery system in the world. Natural gas accounts for approximately 38.5% of the electrical generation[5] and 34% of the total energy consumption in the U.S.[6] The majority of the transmission pipelines in service, approximately 300,000 miles of pipelines made of carbon steel, regulated by the American Petroleum Institute (API), were installed in the 1950s and 1960s[3,4].

Hydrogen in natural gas pipelines has the possibility of negatively affecting the steel pipelines that contain the gas. Hydrogen can be absorbed due to its presence as a transmission gas or due to electrochemical reactions such as corrosion. Regardless of the absorption method, there is potential to have significant negative consequences. Specifically, hydrogen exposure can reduce the mechanical strength and fracture resistance, which is referred to as hydrogen embrittlement (HE)[5]. While there is much debate in the literature as to mechanisms of hydrogen embrittlement, the effect of hydrogen is quantified by the loss of ductility of a material that can result in decreased fracture resistance and subcritical cracking[7]. Hydrogen embrittlement experiments have been carried out in gaseous hydrogen for both API 5L X65[8] and X100[9,10].

Steel grades typically used in transmission pipelines include medium strength API 5L: X52, X56, X60, X65, and X70[4]. High strength steels are known to have higher susceptibility to hydrogen embrittlement[11], while the low strength steels used in distribution mains (API 5L A, B, X42, and X46) are known to not be susceptible to hydrogen embrittlement[1,4]. The medium strength steels, X56 and X65, and high strength steel, X100, studied in this paper are of primary interest as they are either already used extensively in natural gas transmission pipelines[4] or are being considered for use with higher pressure transmission pipelines[12]. This research attempts to assist in the determination of the feasibility of blending hydrogen with natural gas in the existing and proposed transmission pipelines.

EXPERIMENTAL PROCEDURE

The three API 5L steels that are tested in this experiment are either typical for natural gas transmission pipelines (X56 and X65) or being considered for use (X100). The X56 samples were machined from commercial pipes manufactured in 2002 with a yield strength of 61 ksi (422 MPa). The X65 samples were machined from commercial pipes made by Nippon Steel with a yield strength of 71 ksi (491 MPa). The X100 samples were machined from experimental pipes fabricated in the late 1990s with a yield strength of 106 ksi (731 MPa). The manufacturer-provided chemical compositions of the three API 5L carbon steels are displayed in Table 1[13].

Table 1: Composition (wt.%) of API 5L Carbon Steels

Elements	C	Mn	P	S	Al	Cr	Cu	Mo	Nb	Ni	Si	Ti	Fe
X56	0.056	1.09	0.008	0.004	0.03	0.04	0.11	0.01	0.02	0.05	0.21	0.01	Bal.
X65	0.080	1.17	0.009	0.003	-	0.018	0.011	0.001	0.001	0.013	0.2	0.016	Bal.
X100	0.085	1.69	0.0013	<0.001	0.029	0.19	0.14	0.17	0.047	0.24	0.24	0.017	Bal.

The microstructure of the API 5L carbon steels were previously characterized[13] and are displayed in Figure 1. The microstructure of X56 is ferritic with martensitic needle structure within the lattice. The microstructure of X65 is ferritic as well [α-Fe]; however, the grain boundaries contain cementite (Fe_3C) [θ-Fe] precipitates. The microstructure of X100 is primarily fine ferrite and bainite structure (elongated θ-Fe} in a α-Fe matrix [10]).

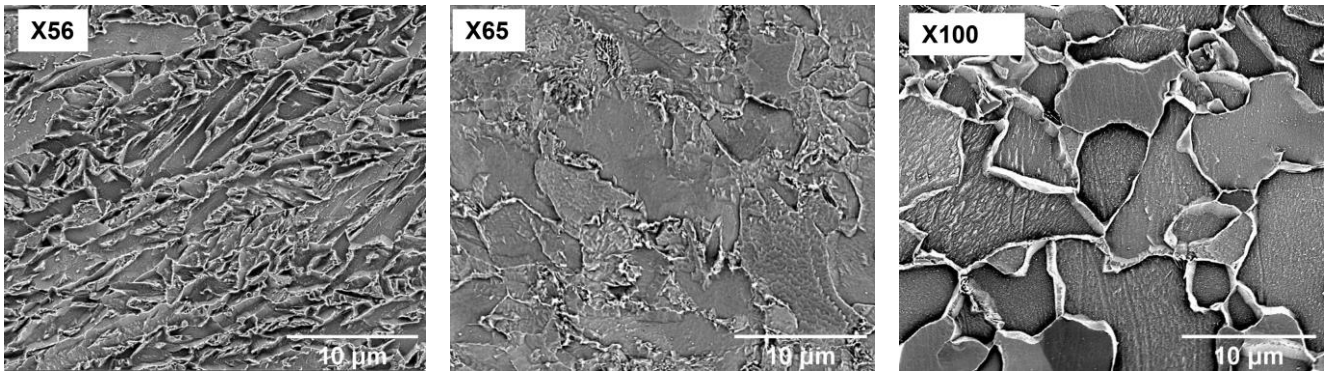

Figure 1: Microstructure of API 5L carbon steels[13].

The hydrogen embrittlement experiments were carried out using specimens printed to dog-bone tensile bar shape, Figure 2a. The mechanical tensile testing samples were machined to 20.3 mm gauge length and 0.89 x 5.84 mm cross-section. A second set of tensile experiments was performed with a stress concentration (SC) to enhance the visualization of hydrogen embrittlement[14]. A SC factor of K_t ~2.7 was created in the dog-bone samples via machining a hole of 0.5 mm, Figure 2b. The reduced cross-section has a blended radius without an undercut, Figure 2. Hydrogen embrittlement testing was performed on samples charged with hydrogen prior to mechanical testing (ex-situ) and charged electrochemically. Therefore, clean surfaces were necessary, and prior to testing, samples were ground using silicon carbide paper (320, 400, and 600 grit), rinsed with isopropanol in an ultrasonic bath and air dried.

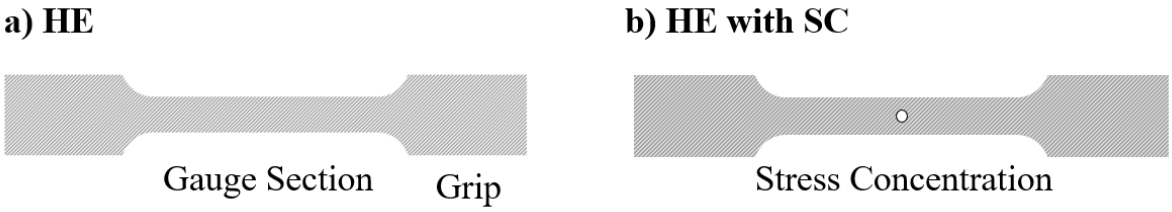

Figure 2: Hydrogen embrittlement dog-bone sample geometry with and without SC.

Specimens were charged galvanostatically (-1 mA/cm^2) in sulfuric acid (0.1 M H_2SO_4) with thiourea (1 g/L CH_4N_2S) for 72 hours. Thiourea is a hydrogen recombination poison which was added to inhibit atomic hydrogen recombination, thereby increasing hydrogen uptake[15]. Hydrogen embrittlement testing was initiated within 15 minutes of removing the sample from the hydrogen charging environment. A 1123 Instron test frame with a 25kN testing capacity and 5800-control system was used for the mechanical testing. The strain rate utilized for testing the specimens was $\dot{\varepsilon} = 6.32 \cdot 10^{-6}\ s^{-1}$ until failure.

In order to compare the effect of hydrogen charging on the API 5L steels, hydrogen-charged samples were compared to as-received samples via mechanical testing plots, plotting stress vs. relative extension. The reduction in failure (RF) was calculated according to Equation 1, where ε is the extension at failure, for both the as-received and the hydrogen embrittled samples. An extensometer was not used for these experiments; therefore, the values are presented as relative extension instead of strain. After failure, the fracture surfaces of the failed samples were imaged using the SEM at 10keV.

$$RF = \frac{\varepsilon_{AR} - \varepsilon_{HE}}{\varepsilon_{AR}} \quad (1)$$

For hydrogen embrittlement experiments, hydrogen is introduced to samples electrochemically via the hydrogen evolution reaction (HER), electrochemically splitting water with a cathodic reaction. HER can be carried out in either alkaline or acidic solutions[16]. The experiments were carried out in an acidic solution, and the global HER reaction is displayed in Equation 2, taking hydrogen ions in solution and forming hydrogen gas. The global mechanism can be broken down between three processes: electrochemical adsorption (Volmer), Equation 3; electrochemical desorption (Heyrovsky), Equation 4; and/or chemical desorption (Tafel), Equation 5[16–20]. Adsorbed hydrogen (H_{ads}) and absorbed hydrogen (H_{abs}) represent hydrogen atoms adsorbed on the external and internal surfaces, respectively. Some hydrogen adsorbed onto the external surface permeate into the specimen by dissolution, becoming absorbed on the internal surface, Equation 6.

Acidic HER

$$2H^+ + 2e^- \overset{Global}{\longleftrightarrow} H_2 \tag{2}$$

$$H^+ + M + e^- \overset{Volmer}{\longleftrightarrow} MH_{ads} \tag{3}$$

$$MH_{ads} + H^+ + e^- \overset{Heyrovsky}{\longleftrightarrow} M + H_2 \tag{4}$$

$$2MH_{ads} \overset{Tafel}{\longleftrightarrow} 2M + H_2 \tag{5}$$

Diffusion

$$MH_{ads} \leftrightarrow MH_{abs} \tag{6}$$

The electrochemical process for acid HER during the hydrogen diffusion experiments can be visualized in Figure 3. With the assistance of an external current, hydrogen ions via the electrochemical Volmer reaction are converted to adsorbed hydrogen. Some of this hydrogen recombines to form hydrogen gas via either the electrochemical Heyrovsky or chemical Tafel reactions. The hydrogen that does not recombine on the HER surface absorbs into the sample and diffuses through the steel. The acidic HER reaction used in the embrittlement experiments can be visualized in Figure 3. The entire steel surface is under HER. Hydrogen ions in the acidic solution are adsorbing onto the surface via the Volmer reaction and recombining to gas via the Heyrovsky and Tafel reactions.

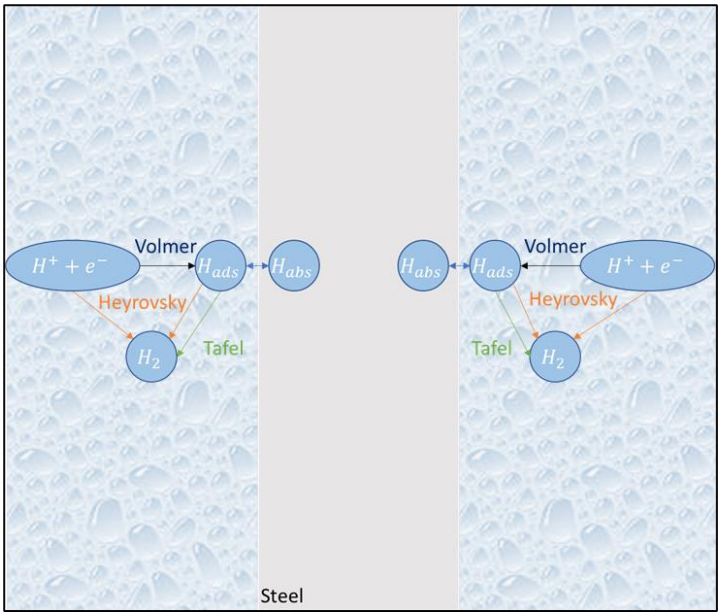

Figure 3: Acidic HER for embrittlement experiments.

RESULTS

The mechanical behavior of the three API 5L steels is displayed in Figure 4. The stress vs. relative extension curves for each alloy (X56, X65, and X100) compare one as-received specimen (solid line) to 3-4 replicate hydrogen-charged specimens (dash/dotted lines). Examining the reduction in failure extension of the hydrogen-charged specimens in comparison to the as-received specimen was used to determine if a hydrogen embrittlement response was detected. A noticeable reduction is expected in samples with a significant hydrogen embrittlement response.

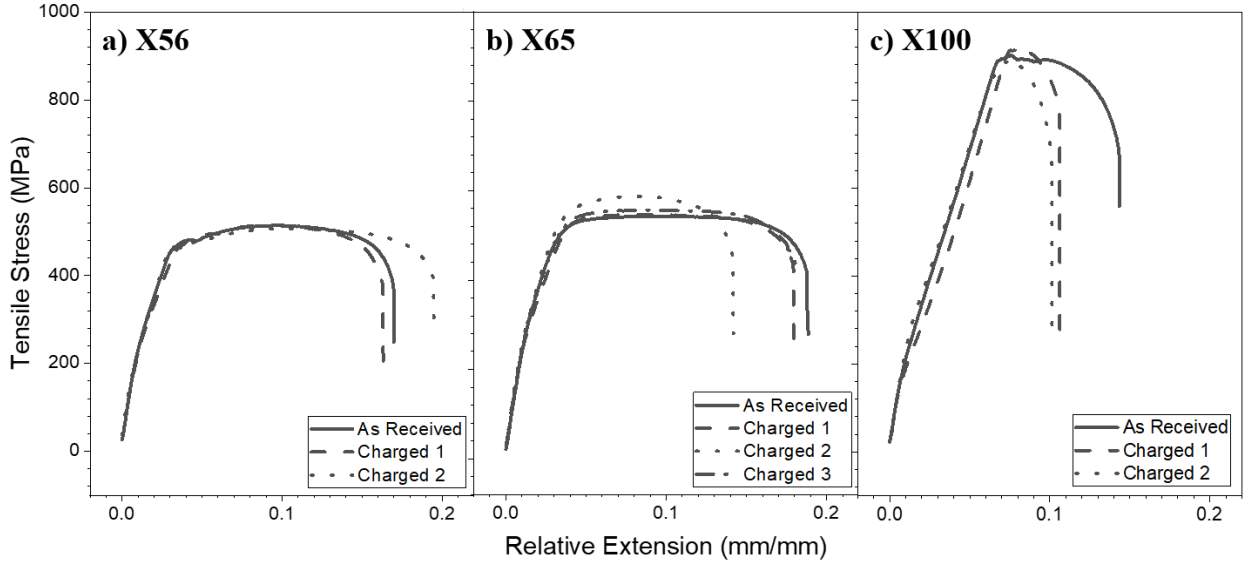

Figure 4: Hydrogen embrittlement stress strain curves comparing as-received specimen to specimens charged for 24 hours in 0.1 M H_2SO_4 with 1 g/L CH_4N_2S at -1 mA/cm^2.

The stress-extension curves for X56, Figure 4a, shows that the yield (YS) and ultimate tensile strength (UTS) are within experimental error between charged and as-received conditions. The relative reduction in extension of the hydrogen-charged X56 specimens, in comparison to the as-received specimen, was -5.4 ± 13.2% according to Equation 1. Though scatter in elongation is expected, there is no measurable indication of embrittlement for X56 with this ex-situ methodology. The stress-extension curves for X65, Figure 4b, shows good conformity of YS and UTS and are within experimental error for the charged and as-received conditions. Though there was one exception as the Charged 2 specimen had slightly larger YS and UTS than the rest of the specimens. The relative reduction in extension of the hydrogen-charged X65 specimens was 10.9 ± 11.9%. Only the X65 Charged 2 specimen showed significant signs of embrittlement. The stress-extension curves for X100, Figure 4c, shows YS and UTS are within experimental error for all conditions. The reduction in relative extension for the hydrogen-charged X100 specimens was 27.6 ± 2.4%.

In conformity with previous research, the majority of the electrochemically generated hydrogen that travelled into the specimens remained near the surface[21]. The long edge of the specimens is where the maximum hydrogen concentration is expected; therefore, Figure 5 shows representative fractographs along that region. Both X56 and X65 show shear lips and shear dimples near the edge of specimens regardless of whether the sample was as-received or hydrogen-charged. This demonstrates that the primary failure mode was ductile. Figure 5d corresponds to the X65 Charged 2 sample that the stress-extension graphs indicate would have the largest degree of embrittlement; however, there were no significant signs of brittle fracture. The X100 as-received samples, Figure 5e, showed shear lips and

ductile dimples, which would indicate primarily ductile failure. The X100 hydrogen-charged fractographs, Figure 5f, revealed mixed brittle and ductile failure response. The primary failure mode appears to be quasi-cleavage with flatter features on the fracture surface.

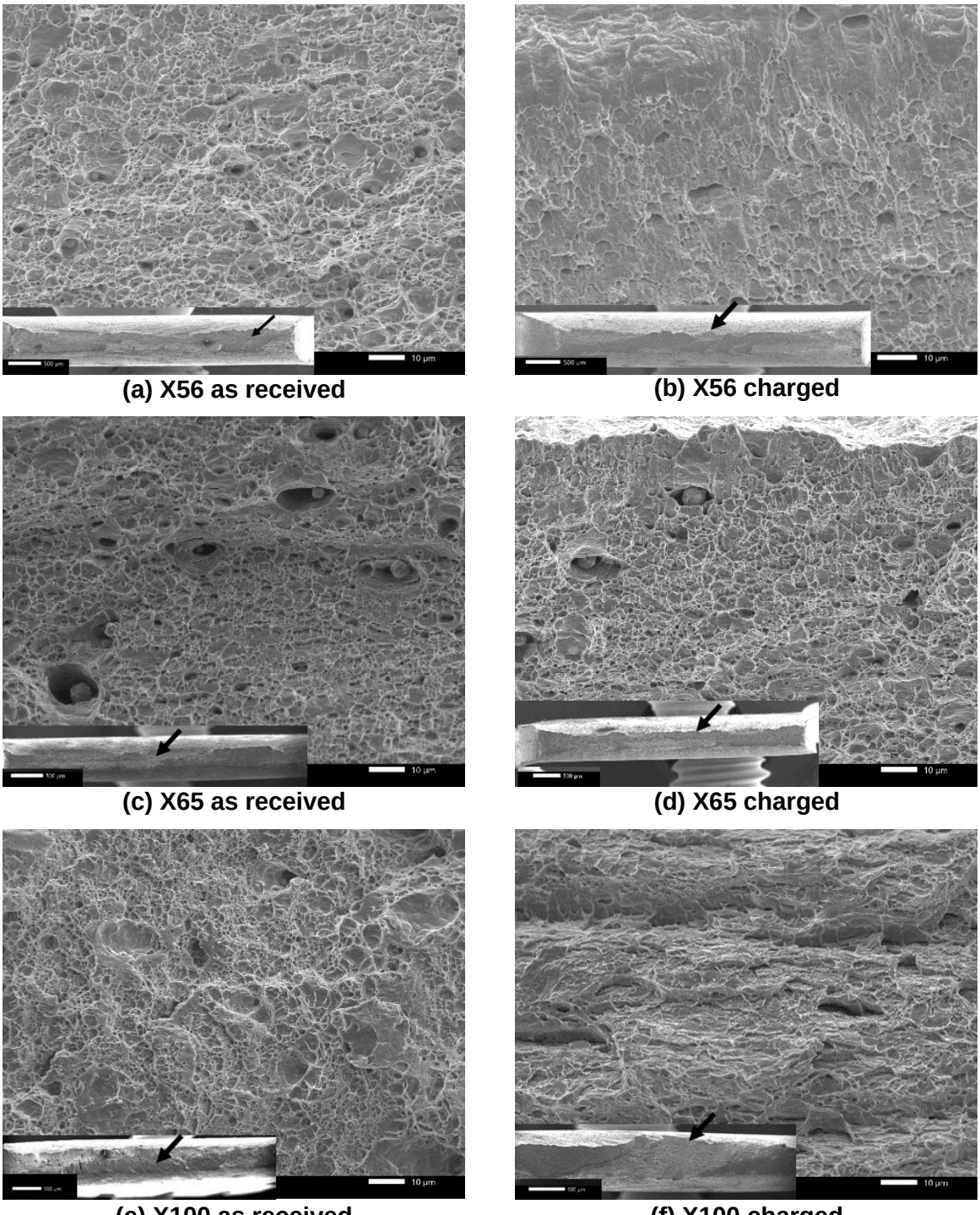

(a) X56 as received **(b) X56 charged**

(c) X65 as received **(d) X65 charged**

(e) X100 as received **(f) X100 charged**

Figure 5: Fracture surface of mechanically tested (a-b) X56, (c-d) X65, and (e-f) X100. (a, c, and e) are as-received API 5L steels and (b, d, and f) are API 5L steels charged with hydrogen before mechanical testing.

The indication for hydrogen embrittlement is defined as a reduction in tensile reduction when comparing hydrogen-charged specimens to as-received specimens. However, Blach et al.[14] has reported a method of using a combination of reduction in notched tensile strength with embrittlement surface fractography in order to determine material sensitivity to hydrogen embrittlement. The API 5L steels in this document were tested with a stress concentration K_t of 2.7 introduced. The notched tensile strength is displayed in Figure 6 and the fractography is displayed in Figure 7. The notched tensile strength tests did not result in significant differences between the hydrogen-charged and as-received specimens for X56, X65, or X100. However, the fracture surfaces did verify signs for hydrogen embrittlement near the stress concentration. The fractography near the stress concentration is displayed in Figure 7. The as-received specimens, Figure 7a, c, and e, display ductile failure. The X56 hydrogen-charged specimen, Figure 7b, shows a mix of shear and cleavage failure up to 15 µm from the stress concentration surface. The replicate X56 hydrogen-charged sample did not contain the mixed behavior and displayed ductile failure. The X65 and X100 hydrogen-charged specimens, Figure 7d, and f, show brittle cleavage features. The change from shear dimples to planar cleavage type failure near the stress concentration is apparent. For X100, the reduction in area near the stress concentration appears to be zero (~750 µm from stress concentration on both sides). The replicates for X65 and X100 repeated this brittle behavior on the fracture surface near the stress concentration.

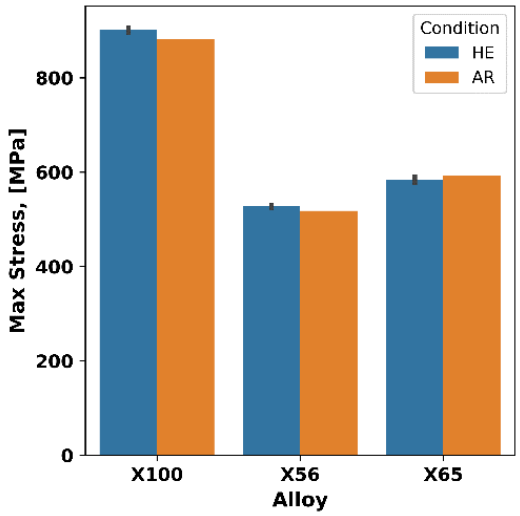

Figure 6: Bar chart of notched tensile strength for API 5L steels with K_t of 2.7. HE denotes hydrogen pre-charged with hydrogen and AR denotes virgin specimens.

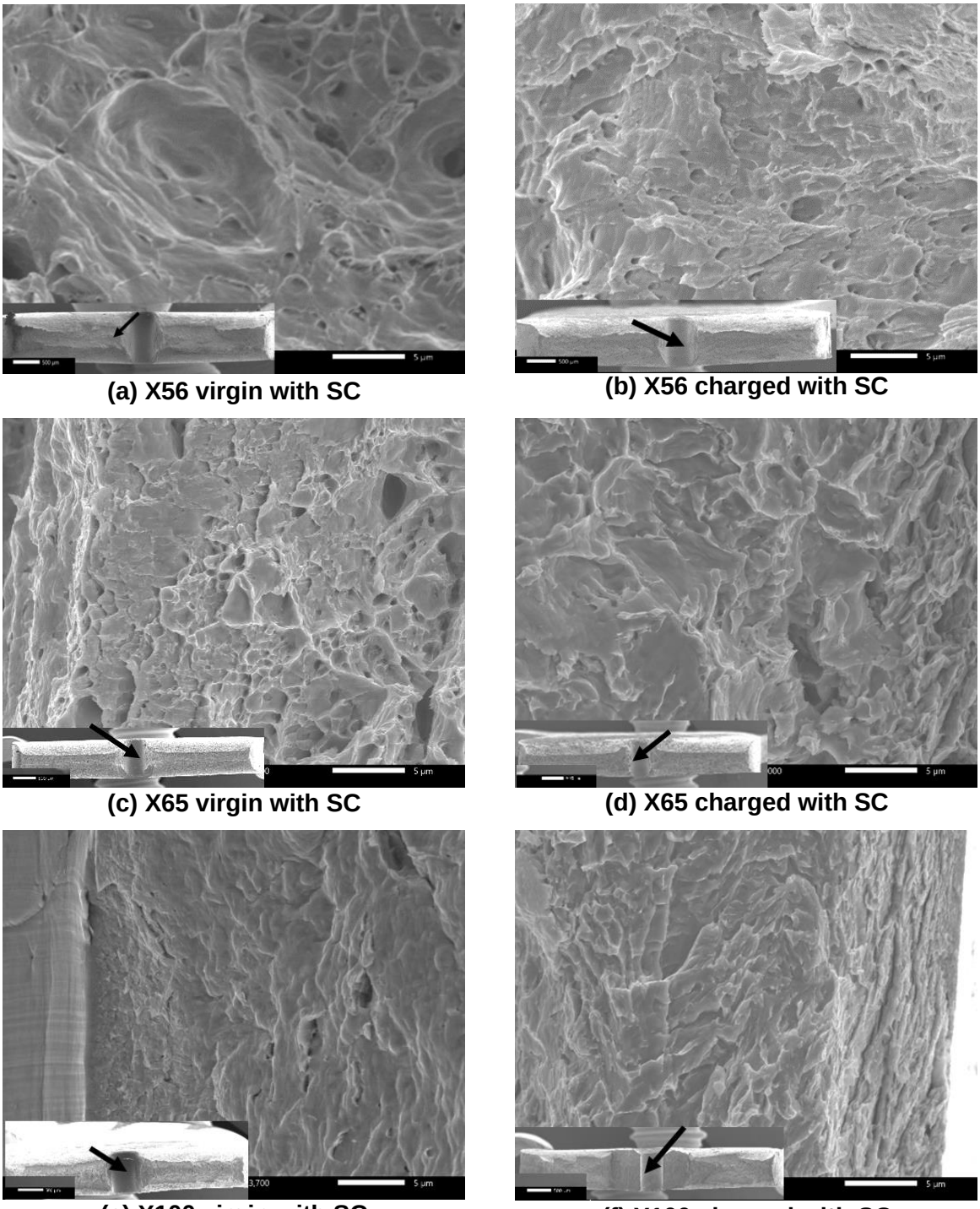

(a) X56 virgin with SC **(b) X56 charged with SC**

(c) X65 virgin with SC **(d) X65 charged with SC**

(e) X100 virgin with SC **(f) X100 charged with SC**

Figure 7: Fracture surfaces of specimens with a stress concentration. A) X56 virgin, B) X56 pre-charged, C) X65 virgin, D) X65 pre-charged, E) X100 virgin, and F) X100 pre-charged.

For the stress-reduction curves the, the loss in specimen ductility and corroborating fracture surfaces can indicate hydrogen embrittlement. The reduction in tensile elongation and the corroborating fracture surface was observed for X100 and indicates clear signs of hydrogen embrittlement for that API 5L steel. Only one of three tests showed any appreciable reduction in tensile elongation for X65 (without corroborating fracture surfaces). No signs of embrittlement were observed for X56.

This research is corroborated by the fact that higher strength steels are generally more susceptible to hydrogen embrittlement[1,4,11]. The strength order precedes highest from X100, X65, to X56. X100 showed clear signs of hydrogen embrittlement, while X65 and X56 showed less indications of hydrogen embrittlement. X65 showed inconsistent hydrogen embrittlement behaviour, which is likely due to the low level of hydrogen penetration typical of ex-situ electrochemical hydrogen generation. In-situ or even high pressure and temperature gaseous charging may provide more consistent embrittlement results for X65[21,22].

Multiple authors have reported that K_t enhances the embrittlement effect of hydrogen[14,23–26]. M. Wang et al.[25] has shown $K_t > 2.1$ have an appreciable effect on notched tensile strength with as little as 0.5 ppmw of diffusible hydrogen. This research also shows enhancement of the embrittlement effects with stress concentrations. All steels from mild X56 to stronger X100 showed evidence of brittle failure near the stress concentration. However, unlike other publications this research did not find a correlating drop in notched tensile strength.

CONCLUSIONS

An appreciable embrittlement response was observed for API 5L X100 steel. A reduction in tensile elongation and change in fracture morphology was observed when comparing hydrogen-charged and as-received specimens. The API 5L X65 steel results were inconsistent. One of the three specimens showed an embrittlement response. The API 5L X56 steel showed no embrittlement response with or without a stress concentration. Specimens with a stress concentration factor showed a change in fracture morphology when charged with hydrogen.

Through hydrogen embrittlement mechanical testing, X56 was demonstrated to have the best qualities. No embrittlement response was found in X56 specimens without a stress concentration. Although X56 was shown to be more resistant to hydrogen embrittlement than the other steels examined, this research also shows the potential for the alloy to be embrittled where stress concentrations exist such as through holes in fastener joints or fatigue-induced crack tips. Based on this research, it was found that X56 can be a candidate for hydrogen pipelines; however, further research, particularly in-situ methodology, is warranted.

ACKNOWLEDGEMENTS

This work was performed in support of the U.S. Department of Energy's (DOE) Fossil Energy and Carbon Management's Methane Mitigation Technology Research Program and executed through the National Energy Technology Laboratory's (NETL) Research & Innovation Center's Natural Gas Infrastructure FWP.

The researchers would like to thank Trevor Godell for machining of specimens, Chris Powell for mechanical testing, and Joe Tylczak and Margaret Ziomek-Moroz for their support and guidance. The authors are grateful to GTI and Joseph Allen Ronevich at Sandia National Laboratories for providing the X56 and X100 carbon steel, respectively.

DISCLAIMER

This project was funded by the United States Department of Energy, National Energy Technology Laboratory, in part, through a site support contract. Neither the United States Government nor any agency thereof, nor any of their employees, nor the support contractor, nor any of their employees, makes any warranty, express or implied, or assumes any legal liability or responsibility for the accuracy, completeness, or usefulness of any information, apparatus, product, or process disclosed, or represents that its use would not infringe privately owned rights. Reference herein to any specific commercial product, process, or service by trade name, trademark, manufacturer, or otherwise does not necessarily constitute or imply its endorsement, recommendation, or favoring by the United States Government or any agency thereof. The views and opinions of authors expressed herein do not necessarily state or reflect those of the United States Government or any agency thereof.

REFERENCES

1. Melaina, M.W., O. Antonia, and M. Penev, "Blending Hydrogen into Natural Gas Pipeline Networks: A Review of Key Issues" (2013), http://www.osti.gov/bridge.
2. National Energy Technology, "NATURAL GAS INFRASTRUCTURE" (n.d.), https://netl.doe.gov/oil-gas/ngi (May 24, 2022).
3. U.S. Energy Information Administration, "Natural Gas Explained: Natural Gas Pipelines" (2021), https://www.eia.gov/energyexplained/natural-gas/natural-gas-pipelines.php (May 24, 2022).
4. Schmura, E., M. Klingenberg, M. Paster, and J. Gruber, "DOE Hydrogen Program: Existing Natural Gas Pipeline Materials and Associated Operational Characteristics" (2005).
5. Rowan, S., D. Kim, Z. Belarbi, A. Wells, D. Hill, B. Dutta, S. Bayham, R. Bergen, and B. Chorpening, "Hydrogen Safety Review for Gas Turbines, SOFC, and High Temperature Hydrogen Production" (2023), https://www.osti.gov/servlets/purl/1969531/.
6. U.S. Energy Information Administration, "U.S. Energy Facts Explained: Consumption and Production" (2021), https://www.eia.gov/energyexplained/us-energy-facts/ (May 24, 2022).
7. Djukic, M.B., V. Sijacki Zeravcic, G.M. Bakic, A. Sedmak, and B. Rajicic, *Eng Fail Anal* 58 (2015): pp. 485–498.
8. Silva, S.C. da, E.A. de Souza, F. Pessu, Y. Hua, R. Barker, A. Neville, and J.A. da Cunha Ponciano Gomes, *Eng Fail Anal* 99 (2019): pp. 273–291.
9. Han, Y.D., R.Z. Wang, H. Wang, and L.Y. Xu, *Int J Hydrogen Energy* 44 (2019): pp. 22380–22393.
10. Ronevich, J.A., C.R. D'Elia, and M.R. Hill, *Eng Fract Mech* 194 (2018): pp. 42–51.
11. Bhadeshia, H.K.D.H., *ISIJ International* 56 (2016): pp. 24–36.
12. Witek, M., *J Nat Gas Sci Eng* 27 (2015): pp. 374–384.
13. Belarbi, Z., L. Teeter, R.E. Chinn, M. Ziomek-Moroz, and O.N. Dogan, "Corrosion Behavior of Transmission Pipeline Steels in Dense-Phase Carbon Dioxide," in AMPP Annual Conference + Expo 2022 (San Antonio, Tx: AMPP, 2022).
14. Blach, J., L. Falat, and P. Ševc, *Eng Fail Anal* 18 (2011): pp. 485–491.
15. Truschner, M., A. Trautmann, and G. Mori, *BHM Berg- Und Hüttenmännische Monatshefte* 166 (2021): pp. 443–449.
16. Lasia, A., *Int J Hydrogen Energy* 44 (2019): pp. 19484–19518.
17. Lu, X., D. Wang, and R. Johnsen, *Electrochim Acta* 421 (2022): p. 140477.
18. Liu, Q., A.D. Atrens, Z. Shi, K. Verbeken, and A. Atrens, *Corros Sci* 87 (2014): pp. 239–258.
19. Bockris, J.O., J. McBreen, and L. Nanis, *Journal of Electrochemical Society* 112 (1965): pp. 1025–1031.
20. Zhang, L., W. Cao, K. Lu, Z. Wang, Y. Xing, Y. Du, and M. Lu, *Int J Hydrogen Energy* 42 (2017): pp. 3389–3398.
21. Lee, S.I., J.M. Lee, S.Y. Lee, H.J. Kim, J.Y. Suh, J.H. Shim, U.B. Baek, S.H. Nahm, J. Lee, and B. Hwang, *Materials Science and Engineering: A* 766 (2019): p. 138367.

22. Wang, D., A.B. Hagen, P.U. Fathi, M. Lin, R. Johnsen, and X. Lu, *Materials Science and Engineering A* 860 (2022).
23. Walter, R.J., and W.T. Chandler, *Materials Science and Engineering* 8 (1971): pp. 90–97.
24. Hardie, D., and E. Liu, *Corros Sci* 38 (1996): pp. 721–733.
25. Wang, M., E. Akiyama, and K. Tsuzaki, *Materials Science and Engineering A* 398 (2005): pp. 37–46.
26. Steinman, J.B., H.C. VanNess, and G.S. Ansel, *Welding Journal, Welding Research Supplement* 44 (1965): pp. 221–224.